Article

Cell Reports

The CST Complex Mediates End Protection at Double-Strand Breaks and Promotes PARP Inhibitor Sensitivity in BRCA1-Deficient Cells

Graphical Abstract

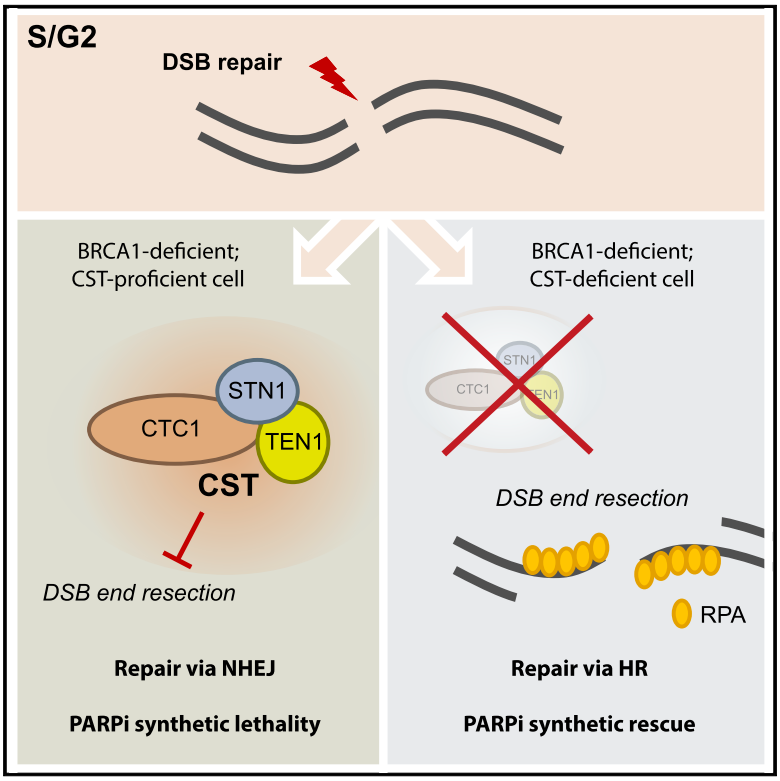

Highlights

- PARP inhibitor resistance screens independently identify loss of CTC1 as major hit
- The CST complex promotes PARP inhibitor sensitivity in BRCA1-deficient cells
- Depletion of CTC1 restores end resection in BRCA1-deficient cells
- CTC1 facilitates double-strand break repair via canonical non-homologous end joining

Authors

Marco Barazas, Stefano Annunziato, Stephen J. Pettitt, ..., Christopher J. Lord, Jos Jonkers, Sven Rottenberg

Correspondence

j.jonkers@nki.nl (J.J.), sven.rottenberg@vetsuisse.unibe.ch (S.R.)

In Brief

Using CRISPR/SpCas9-based loss-of-function screens, Barazas et al. show that loss of the CTC1-STN1-TEN1 (CST) complex promotes PARP inhibitor resistance in BRCA1-deficient cells. Mechanistically, the CST complex maintains double-strand break end stability in addition to its role in protecting telomeric ends.

Barazas et al., 2018, Cell Reports *23*, 2107–2118
May 15, 2018
https://doi.org/10.1016/j.celrep.2018.04.046

CellPress

Cell Reports
Article

The CST Complex Mediates End Protection at Double-Strand Breaks and Promotes PARP Inhibitor Sensitivity in BRCA1-Deficient Cells

Marco Barazas,[1] Stefano Annunziato,[1] Stephen J. Pettitt,[2] Inge de Krijger,[3] Hind Ghezraoui,[4] Stefan J. Roobol,[5,6] Catrin Lutz,[1] Jessica Frankum,[2] Fei Fei Song,[2] Rachel Brough,[2] Bastiaan Evers,[7] Ewa Gogola,[1] Jinhyuk Bhin,[1,7] Marieke van de Ven,[1,8] Dik C. van Gent,[5] Jacqueline J.L. Jacobs,[3] Ross Chapman,[4] Christopher J. Lord,[2] Jos Jonkers,[1,*] and Sven Rottenberg[1,9,10,*]

[1]Division of Molecular Pathology, Oncode Institute, the Netherlands Cancer Institute, 1066CX Amsterdam, the Netherlands
[2]The CRUK Gene Function Laboratory and Breast Cancer Now Toby Robins Research Centre, The Institute of Cancer Research, London SW3 6JB, UK
[3]Division of Oncogenomics, the Netherlands Cancer Institute, 1066CX Amsterdam, the Netherlands
[4]Genome Integrity Laboratory, Wellcome Centre for Human Genetics, University of Oxford, Oxford OX3 7BN, UK
[5]Department of Genetics, Erasmus University Medical Center, Rotterdam, the Netherlands
[6]Department of Radiology and Nuclear Medicine, Erasmus University Medical Center, Rotterdam, the Netherlands
[7]Division of Molecular Carcinogenesis, the Netherlands Cancer Institute, 1066CX Amsterdam, the Netherlands
[8]Mouse Clinic for Cancer and Aging Research (MCCA), Preclinical Intervention Unit, the Netherlands Cancer Institute, 1066CX Amsterdam, the Netherlands
[9]Institute of Animal Pathology, Vetsuisse Faculty, University of Bern, Bern, Switzerland
[10]Lead Contact
*Correspondence: j.jonkers@nki.nl (J.J.), sven.rottenberg@vetsuisse.unibe.ch (S.R.)
https://doi.org/10.1016/j.celrep.2018.04.046

SUMMARY

Selective elimination of BRCA1-deficient cells by inhibitors of poly(ADP-ribose) polymerase (PARP) is a prime example of the concept of synthetic lethality in cancer therapy. This interaction is counteracted by the restoration of BRCA1-independent homologous recombination through loss of factors such as 53BP1, RIF1, and REV7/MAD2L2, which inhibit end resection of DNA double-strand breaks (DSBs). To identify additional factors involved in this process, we performed CRISPR/SpCas9-based loss-of-function screens and selected for factors that confer PARP inhibitor (PARPi) resistance in BRCA1-deficient cells. Loss of members of the CTC1-STN1-TEN1 (CST) complex were found to cause PARPi resistance in BRCA1-deficient cells *in vitro* and *in vivo*. We show that CTC1 depletion results in the restoration of end resection and that the CST complex may act downstream of 53BP1/RIF1. These data suggest that, in addition to its role in protecting telomeres, the CST complex also contributes to protecting DSBs from end resection.

INTRODUCTION

The synthetic lethal interaction between BRCA1 deficiency and poly(ADP-ribose) polymerase (PARP) inhibition is a well-established therapeutic paradigm with encouraging response rates in the clinic (Lord and Ashworth, 2017). This has resulted in the recent regulatory approval of three PARP inhibitors (PARPis) for the treatment of serous ovarian cancers and one PARPi, olaparib, for the treatment of *BRCA*-mutated, HER2-negative breast cancers. Moreover, the BRCA-PARP paradigm might be extended beyond breast and ovarian cancer because recent clinical studies indicate that a subset of prostate cancers harbor a homologous recombination (HR) defect and, hence, might benefit from olaparib treatment (Mateo et al., 2015; Pritchard et al., 2016).

Despite this success, long-lasting clinical response rates in patients with advanced disease are limited by the development of resistance, the mechanisms of which have not been fully elucidated. A major class of resistance mechanisms centers on re-expression of functional BRCA1 or BRCA2 protein, either through promoter demethylation, genetic reversion, or gene fusions (Patch et al., 2015; Swisher et al., 2008; Ter Brugge et al., 2016). However, our previous work also identified the existence of additional BRCA1-independent resistance mechanisms in the *K14cre;Brca1$^{F/F}$;p53$^{F/F}$* (KB1P) genetically engineered mouse model of hereditary breast cancer (Liu et al., 2007). In this model, re-expression of functional BRCA1 is excluded because of the large, engineered, intragenic *Brca1* deletion, which spans multiple exons. Despite the absence of functional BRCA1 restoration, KB1P tumors acquired resistance to PARPi treatment. In addition to activation of the P-glycoprotein drug efflux transporter (Rottenberg et al., 2008), the BRCA1-independent resistance mechanisms in KB1P tumors predominantly involved the partial restoration of HR activity through re-wiring of the DNA damage response (DDR); for example, by loss of 53BP1 (Bouwman et al., 2010; Bunting et al., 2010; Jaspers et al., 2013). These seminal findings have spurred a number of studies in which additional downstream antagonists of end resection were identified, including RIF1 (Chapman et al., 2013; Di Virgilio et al., 2013; Escribano-Díaz

et al., 2013; Zimmermann et al., 2013) and REV7/MAD2L2 (Boersma et al., 2015; Xu et al., 2015). However, the currently known resistance factors cannot explain all PARPi-resistant cases, suggesting that additional proteins functioning in this pathway remain to be identified. Moreover, although the loss of resection antagonists partially restores end resection of DNA double-strand breaks (DSBs), none of these factors have direct functions in DNA metabolism, raising the question of how DNA metabolism at DSBs might be altered to stimulate end resection.

The function of the 53BP1 pathway is not exclusive to canonical DSB repair, but it also acts on telomeres (Panier and Boulton, 2014). Because telomere ends resemble DSBs located at chromosomal termini, cells have evolved several mechanisms to protect telomeres from DSB end processing and chromosome end-to-end fusions (Sfeir and de Lange, 2012). Mammalian telomeres consist of TTTAGG repeats ending with a single-strand G-rich overhang. The single-stranded DNA (ssDNA) overhang is crucial in telomere maintenance because it is required for the formation of the T-loop structure (Makarov et al., 1997; McElligott and Wellinger, 1997). Notably, excessive resection of telomere ends is inhibited by the action of the shelterin complex and by the 53BP1 pathway (Lazzerini-Denchi and Sfeir, 2016; Sfeir and de Lange, 2012).

Besides the mechanisms that have evolved to protect telomeric overhangs from excessive processing, it has recently been shown that the RPA-like CTC1-STN1-TEN1 (CST) complex is able to localize to telomeric ssDNA and mediate a fill-in reaction executed by polymerase-alpha (POLA) to buffer resection activity (Feng et al., 2017; Miyake et al., 2009; Wu et al., 2012). Notably, it was demonstrated that the binding of the CST complex to ssDNA is not particularly sequence-specific, although a partial preference for G-rich regions has been described (Hom and Wuttke, 2017; Miyake et al., 2009). Additionally, CST components do not localize exclusively to telomeres (Miyake et al., 2009). This might argue that the CST complex also has non-telomeric functions.

In this study, three independent forward genetic CRISPR/SpCas9-based loss-of-function screening approaches were employed to identify factors that induce PARPi resistance in BRCA1-deficient cells. Together, these screens identified that defects in *Ctc1*, or its CST complex members *Stn1* or *Ten1*, suppress the synthetic lethal interaction between BRCA1 and PARP inhibition. Inactivation of CTC1 is sufficient to drive PARPi resistance *in vivo*. Depletion of CTC1 increased end resection activity and subsequently restored RAD51 focus formation upon ionizing radiation (IR)-induced DNA damage, providing a mechanistic basis for these observations. Moreover, the CST complex facilitates canonical non-homologous end joining (c-NHEJ)-driven repair. Together, these data demonstrate that the CST complex plays a more global role in DNA repair beyond the protection of telomeres.

RESULTS

Forward Genetic CRISPR/SpCas9 Screens Identify Selective Enrichment for Loss of CTC1 during PARPi Treatment in BRCA1-Deficient Cells

To identify factors that modulate the synthetic lethal interaction between BRCA1 and PARP, we carried out three independent forward genetic loss-of-function CRISPR/SpCas9 screens (Figure 1). All screens were analyzed by harvesting cells before and after PARPi treatment, after which single guide RNA (sgRNA) sequences were amplified from genomic DNA by PCR and analyzed by next-generation sequencing. The screening data were processed by the model-based analysis of genome-wide CRISPR-Cas9 knockout (MAGeCK) or the drugZ algorithm (Li et al., 2014; Wang et al., 2017), and the results were sorted on positive selected gene ranks to allow comparison across screens. Additional experimental details are provided in the Supplemental Experimental Procedures.

The first PARPi resistance screen was performed in SpCas9-expressing KB1P-G3 mouse mammary tumor cells (Jaspers et al., 2013) using a custom-made lentiviral sgRNA library targeting 1,752 DDR-related genes (Table S1) cloned into the doxycycline-inducible pLenti-sgRNA-tetR-T2A-PuroR vector (Prahallad et al., 2015). The screen was performed at 100× coverage, and cells were selected with two different PARPis, olaparib and AZD2461 (Oplustil O'Connor et al., 2016), at the approximate inhibitory concentration 90 (IC90) for 14 days (Figure 1A). Although sgRNAs targeting *Tp53bp1* were deliberately removed from the library to avoid the possibility that this potent PARPi resistance factor might obscure the effects of other genes, its upstream regulatory factor *Rnf8* scored among the top genes (Figure 1B).

The second PARPi resistance screen was performed in SpCas9-expressing *Brca1*$^{-/-}$;*Trp53*$^{-/-}$ mouse embryonic stem cells (mESCs) infected with a genome-wide lentiviral sgRNA library targeting 19,150 genes (Koike-Yusa et al., 2014). The screen was performed at 75× coverage in two independent transductions, and cells were selected with olaparib at a concentration of 15 nM for 10 days. As expected, *Tp53bp1* and *Rnf8* scored among the top genes and ranked #1 and #15, respectively (Figure 1C).

A third PARPi resistance screen was performed in *BRCA1*^{2288delT} mutant SUM149PT human breast cancer cells (Elstrodt et al., 2006). SUM149PT cells expressing doxycycline-inducible SpCas9 were lentivirally infected with a genome-wide sgRNA library targeting 18,010 genes (Tzelepis et al., 2016). This screen was performed at 1,000× coverage, and cells were selected in the presence of doxycycline plus 100 nM talazoparib for 2 weeks. The screen was dominated by sgRNAs targeting *PARP1*, the drug target of talazoparib. Although PARP1 loss is expected to be lethal in BRCA1-deficient cells, the selection for PARP1 loss in SUM149PT cells might be attributed to residual BRCA1 activity, which might enable cell survival in the absence of PARP1 (Pettitt et al., 2017; Wang et al., 2016). Moreover, *TP53BP1* scored among the top enriched genes and ranked #7 (Figure 1D).

The results from these three independent screens were collated to identify consistent outliers. The top 20 genes were selected from the DDR-focused library screen in KB1P-G3 cells. Because the genome-wide libraries contain about 10-fold more genes than the DDR-focused library, the top 200 genes were selected from the mESC and SUM149PT screens, and these were plotted in a Venn diagram (Figure 1E). Notably, *Ctc1* was the only gene that consistently scored in all three screens (ranked #10, #39, and #39 in the KB1P-G3, mESC, and

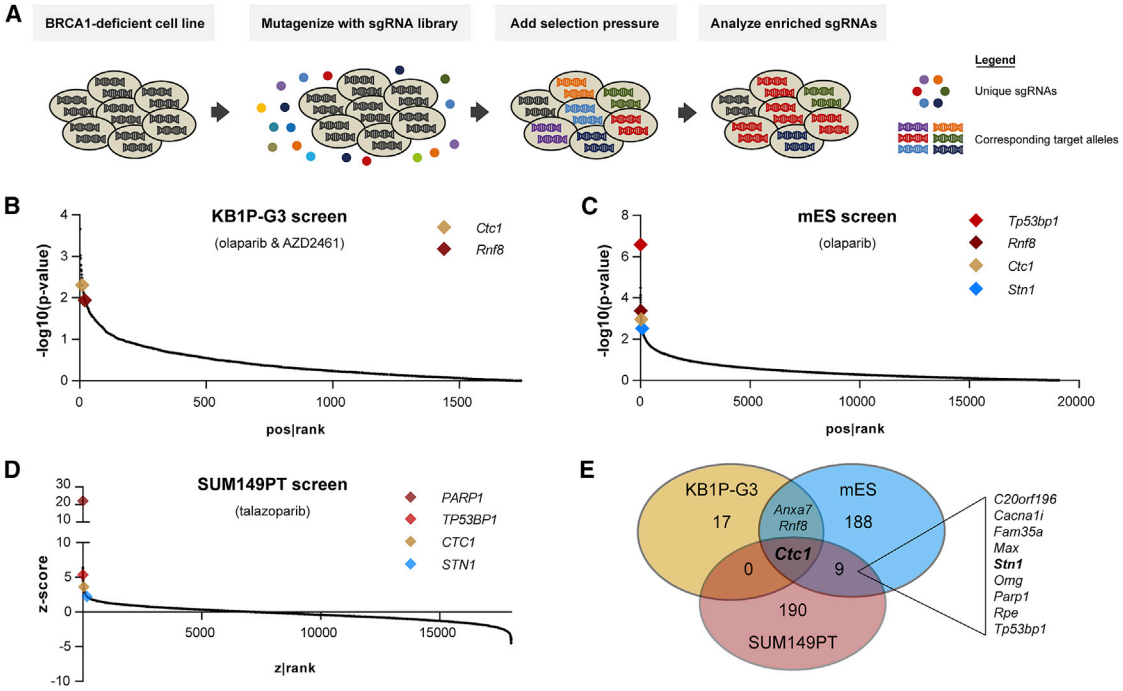

Figure 1. Multiple Independent CRISPR/SpCas9 Loss-of-Function Screens Identify CTC1 as a Driver of PARPi Resistance in BRCA1-Deficient Cells

(A) Schematic overview of the screening approach utilized across the different screens. Each screen was performed on a different cell line and screened with a different library, which is indicated per screen.

(B) SpCas9-expressing KB1P-G3 cells were screened with a DNA damage response (DDR)-focused library at 100× coverage. Cells were plated for clonogenic growth in the presence of olaparib (75 nM) or AZD2461 (250 nM) for 14 days, and sgRNA abundance in treated populations was compared with the starting population using MAGeCK software. Gene-based p values were log-transformed and plotted based on the positive rank (enrichment). Each dot represents a unique gene.

(C) *Brca1*$^{-/-}$;*Trp53*$^{-/-}$ mouse embryonic stem cells (mESCs) were screened with a genome-wide library in two independent transductions at 75× coverage. After 10 days of culture in the presence of olaparib (15 nM), treated populations were compared with the untreated population using MAGeCK software. Gene based p values were log-transformed and plotted based on the positive rank (enrichment). Each dot represents a unique gene.

(D) A derivative of the *BRCA1* mutant SUM149PT human triple-negative breast tumor cell line carrying a doxycycline-inducible SpCas9 expression construct was lentivirally infected with a genome-wide guide RNA library at more than 1,000× coverage. Cells were cultured in the presence of doxycycline plus 100 nM talazoparib for 2 weeks. The sgRNA abundance in treated populations was compared with the starting population using drugZ. Gene-based *Z* scores were log-transformed and plotted based on the positive z-rank (enrichment). Each dot represents an individual gene.

(E) The top 20 genes in the KB1P-G3 screen and the top 200 genes in the mESC and SUM149PT screens were selected and plotted in a Venn diagram to identify consistent outliers.

SUM149PT screens, respectively). Moreover, *Stn1* (also known as *Obfc1*) scored in two of three screens. These results caught our attention because both CTC1 and STN1 are members of the CST complex. Although the CST complex has known functions in telomere metabolism, these PARPi resistance screens might point toward non-telomeric functions of the CST complex. Because *Ctc1* was a top hit in all three independent screens in both mouse and human cells, we prioritized this gene for further validation.

Depletion of CTC1 Suppresses the Synthetic Lethal Interaction between BRCA1 Deficiency and PARP Inhibition

To validate the effect of CTC1 on PARPi sensitivity in BRCA1-deficient cells, we transfected KB1P-G3 cells with pX330 vectors containing three sgRNAs targeting a putative oligonucleotide-binding (OB) fold domain of *Ctc1* (Figure 2A). The polyclonal targeted populations were efficiently modified for the target site (Figures 2B–2D), as shown by TIDE (tracking of insertions or deletions [indels] by decomposition) analysis (Brinkman et al., 2014). These populations were subsequently treated with olaparib (75 nM) or AZD2461 (250 nM), the same concentrations as used for the screen. As expected, parental KB1P-G3 cells or KB1P-G3 cells targeted by a non-targeting sgRNA (sgNT) showed high sensitivity to PARPi treatment. In contrast, *Ctc1*-targeted cells showed resistance to treatment, indicating that depletion of CTC1 suppresses the synthetic lethal interaction between BRCA1 deficiency and PARP inhibition (Figures 2E and F). This could not be attributed to an effect on cell proliferation because we observed no difference in the doubling time upon depletion of CTC1 (Figure 2G).

We next investigated whether *Ctc1*-mutated cells would be specifically selected out from a mixed population by prolonged PARPi treatment. A competition assay was performed in which

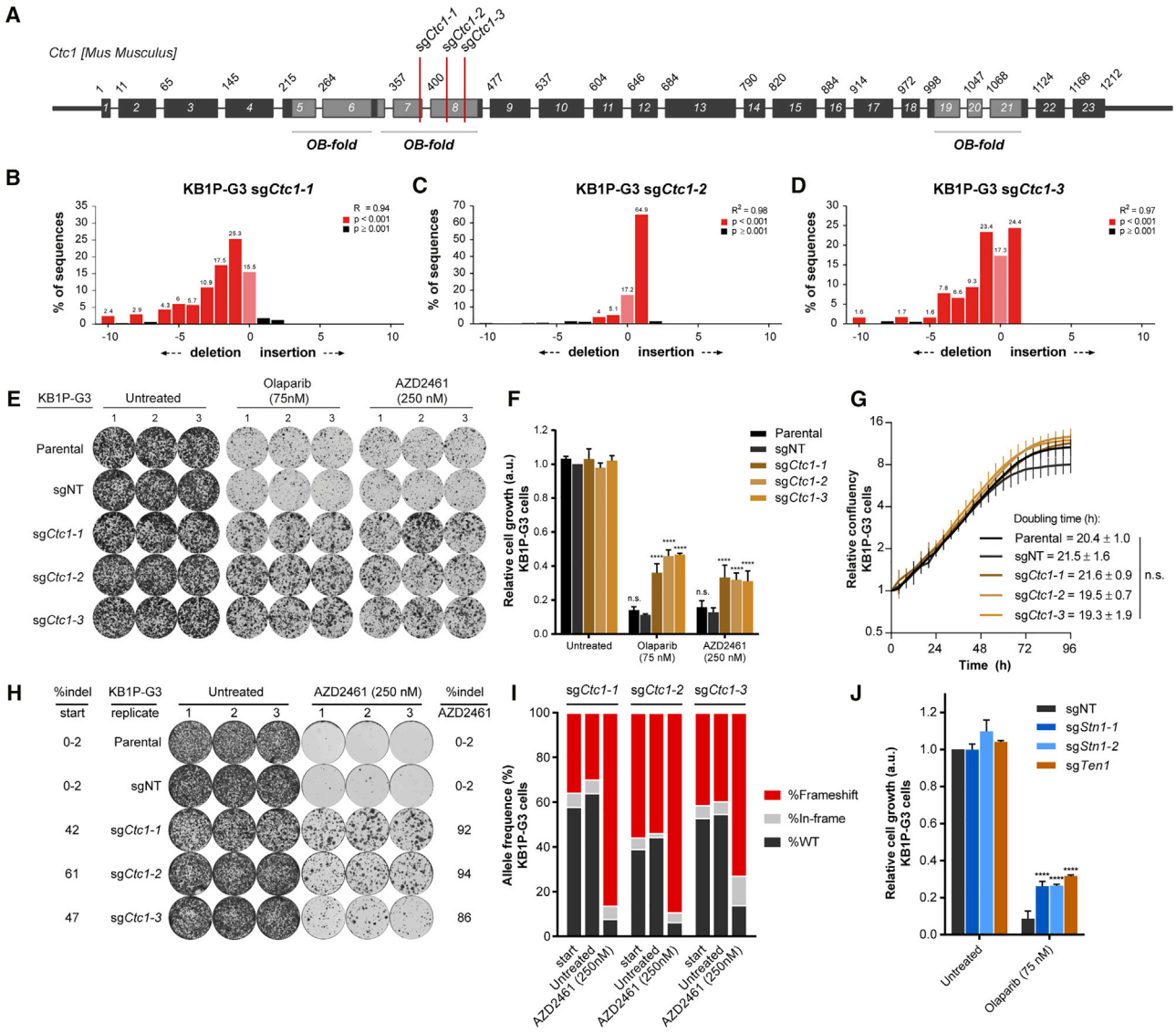

Figure 2. Depletion of CTC1 Suppresses the Synthetic Lethal Interaction between BRCA1 Deficiency and PARP Inhibition

(A) Schematic overview of the *Ctc1* gene, in which putative OB fold domains and sgRNA target locations are indicated (adapted from Miyake et al., 2009).

(B–D) KB1P-G3 cells were transfected with pX330puro vectors containing the indicated sgRNAs, and the target region was PCR-amplified to verify allele modification using TIDE software.

(E) The indicated *Ctc1*-mutated KB1P-G3 cell lines were plated for clonogenic growth upon olaparib (75 nM) or AZD2461 (250 nM) treatment. Three independent experiments were performed, and each condition was plated in triplicate. One representative well per condition is shown for each independent experiment.

(F) Quantification of crystal violet staining in (E). Data were plotted relative to the growth of untreated sgNT cells and are presented as mean ± SD (n = 3 independent experiments). Significance was calculated by two-way ANOVA with Dunnett's multiple comparisons test (****adjusted p = 0.0001).

(G) Relative cell proliferation was determined by IncuCyte Zoom Live – Cell Analysis System measurements. Each data point represents the average of three independent experiments, and in each experiment, six replicate wells were measured and averaged. Data represent mean ± SD (n = 3). Doubling times (exponential growth equation) were calculated using GraphPad software, and significance was calculated by one-way ANOVA with Dunnett's multiple comparisons test.

(H and I) SpCas9-expressing KB1P-G3 cells were transduced with doxycycline-inducible pLenti-sgRNA-tetR-T2A-PuroR vectors containing the indicated sgRNAs. Polyclonal populations were plated for clonogenic growth with or without AZD2461 (250 nM) (H). Cells were passaged every 10 days for a total of three times. At the endpoint, wells were fixed and stained with crystal violet, and allele distributions were determined from each condition using TIDE software (I).

(J) KB1P-G3 cells were transfected with pX330puro vectors containing sgRNAs targeting *Stn1* and *Ten1* and cultured in the presence or absence of 75 nM olaparib as in (E). Data were analyzed as in (F) and reflect at least two independent experiments.

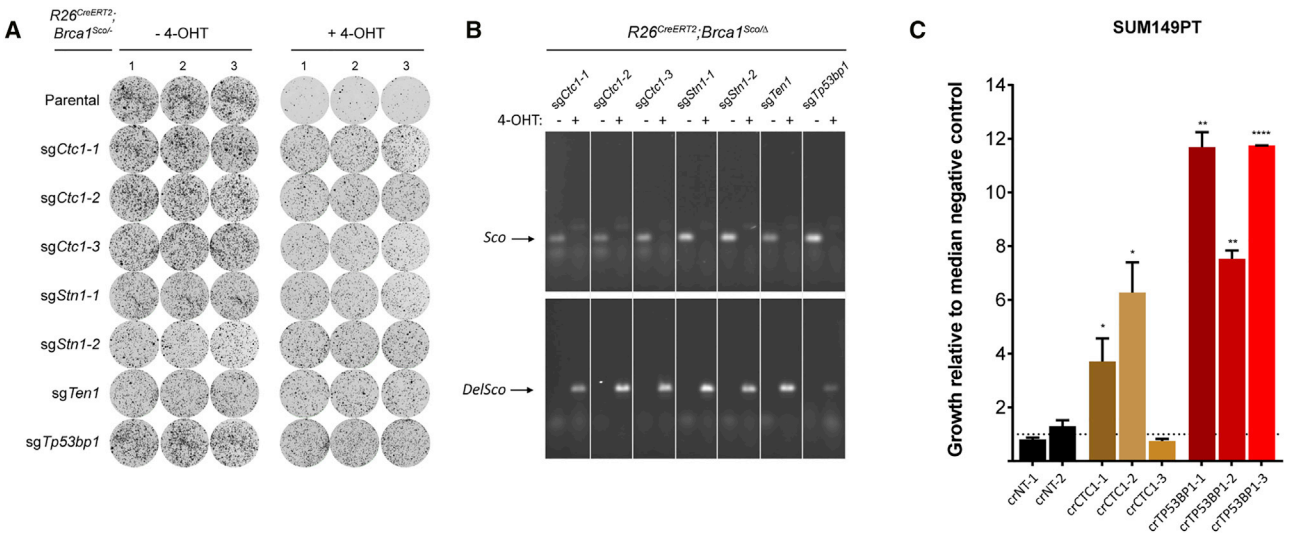

Figure 3. Loss of CST Complex Members Induces PARPi Resistance in BRCA1-Deficient mESCs and SUM149PT Breast Cancer Cells

(A) *Ctc1*, *Stn1*, and *Ten1* were targeted in R26^{CreERT2};Brca1$^{SCo/\Delta}$ mESCs using pLentiCRISPRv2 vectors. Following transduction and selection, the *Brca1-Sco* allele was recombined by activation of CreERT2 via addition of 4-OHT, after which cells were plated out for clonogenic growth. Cells were fixed and stained with crystal violet.

(B) *Brca1* alleles from surviving populations were PCR-amplified using specific primers to detect *Brca1*^{Sco} (*Sco*) and recombined *Brca1*$^{\Delta Sco}$ (*DelSco*) alleles.

(C) *BRCA1*-mutant SUM149PT cells were transfected with the EditR CRISPR system, and the indicated CRISPR RNA (crRNA) and then continuously cultured in the presence of 50 nM talazoparib over a 14-day period, at which point cell viability was estimated by use of CellTiter-GLo reagent. Median effects from three independent experiments are shown. Error bars represent SEM. *p = 0.0415 and 0.0201, respectively; **p = 0.0013 and 0.0011, respectively; ****p = < 0.0001; unpaired two-tailed Student's t test.

the evolution of polyclonal populations was monitored by the TIDE algorithm to quantify changes in allele distributions. sgRNAs were cloned in the pLenti-sgRNA-tetR-T2A-Puro vector and introduced in SpCas9-expressing KB1P-G3 cells by lentiviral transduction. The population was mutagenized by doxycycline-induced expression of the sgRNA for 5 days, after which cells were plated without doxycycline for clonogenic growth. After 10 days of culture in the presence or absence of AZD2461, the cells were harvested and re-plated at equal amounts every 10 days for an additional two rounds, resulting in a total treatment duration of 30 days. Although non-transduced cells or cells transduced with a non-targeting sgRNA were effectively killed by this prolonged treatment, *Ctc1*-targeted cells survived (Figure 2H). This coincided with an enrichment of *Ctc1* frameshift mutations compared with untreated populations, which were kept in culture for the same duration (Figure 2I).

To study whether this effect is CTC1-specific or a feature of the CST complex, we genetically inactivated the other two CST complex members *Stn1* and *Ten1*, and treated these cells with olaparib under the same conditions as used for *Ctc1*. CRISPR/SpCas9-mediated disruption of *Stn1* or *Ten1* also induced PARPi resistance, recapitulating the effect of *Ctc1* (Figure 2J). This is consistent with the identification of STN1 in the PARPi resistance screens (Figure 1E) and shows that PARPi sensitivity is modulated by all CST complex members rather than CTC1 alone.

These data were corroborated in *Brca1*$^{-/-}$*;Trp53*$^{-/-}$ mESCs in which CRISPR/SpCas9-assisted inactivation of *Ctc1* increased survival upon olaparib treatment, which was accompanied by a selection for frameshifting alleles (Figures S1A and S1B). Furthermore, we targeted the CST complex members in R26^{CreERT2};Brca1$^{SCo/\Delta}$ mESCs, which harbor a selectable conditional Brca1^{Sco} allele that can be inactivated by CreERT2 through the addition of 4-hydroxytamoxifen (4-OHT) (Bouwman et al., 2010). Although 4-OHT-induced inactivation of BRCA1 caused lethality in untransduced R26^{CreERT2};Brca1$^{SCo/\Delta}$ mESCs, clonal outgrowth was observed for cells depleted of CTC1, STN1, or TEN1 (Figure 3A). Complete switching of the conditional *Brca1*^{Sco} allele in the surviving population was confirmed by PCR, ruling out that clonal outgrowth was due to a non-recombined *Brca1*^{Sco} allele (Figure 3B). Finally, depletion of CTC1 in SUM149PT cells enhanced cell survival in the presence of talazoparib, as did depletion of 53BP1 (Figure 3C), confirming that this effect was not restricted to mouse cells.

In summary, we confirmed that the CST complex promotes PARPi-induced cell lethality in BRCA1-deficient cells. We therefore looked at the role of the CST complex in preventing global DNA damage, focusing on CTC1.

CTC1 Antagonizes End Resection at Non-Telomeric DSBs

During the repair of DSBs, a critical decision is made between initiating repair via NHEJ or via HR, which both require distinct end processing. This decision is tightly balanced by end protection factors, such as 53BP1 or RIF1, which antagonize resection to direct repair via NHEJ, and BRCA1, which promotes end resection to direct repair via HR (Chapman et al., 2013; Daley and Sung, 2014; Escribano-Díaz et al., 2013; Feng et al., 2015;

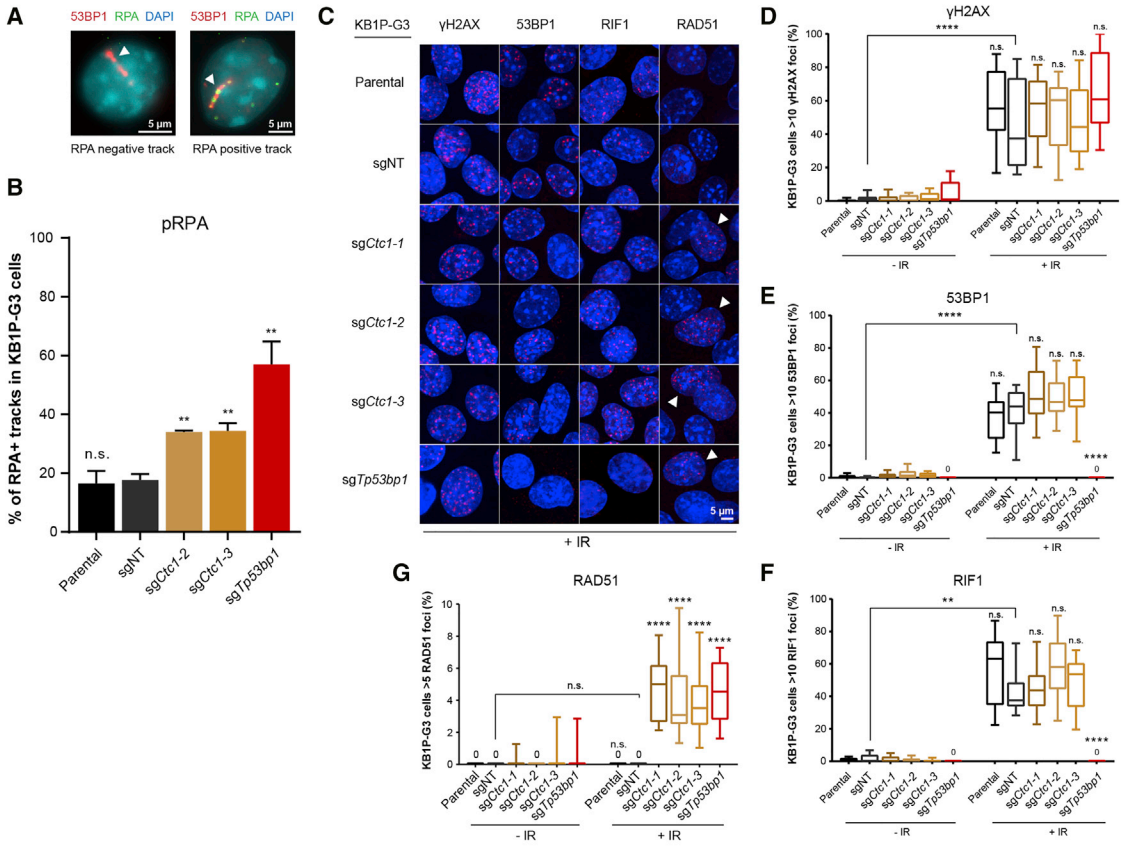

Figure 4. CTC1 Functions as a Resection Antagonist on Non-telomeric DSBs

(A and B) CTC1 depletion induces RPA-coated ssDNA overhangs at sites of DNA damage in BRCA1-defient KB1P cells.

(A) Representative images of RPA-negative and RPA-positive 53BP1-labeled alpha tracks in the indicated CRISPR/SpCas9-targeted KB1P-G3 cells (highlighted by the white arrowheads). Scale bars represent 5 μm.

(B) RPA co-localization was quantified 1 hr after irradiation with an Americium-241 (^{241}Am) point source. The experiment was performed three times, and in each independent experiment, a minimum of 100 tracks were analyzed. Data are plotted as mean ± SEM. Significance was calculated by unpaired two-tailed Student's t test (**$p < 0.01$).

(C and G) CTC1 depletion restores formation of DNA damage-induced RAD51 foci in BRCA1-deficient cells.

(C) Representative confocal images of CRISPR/SpCas9-expressing KB1P-G3 cells targeted with the indicated sgRNAs. Cells were stained 3 hr after 10 Gy of ionizing radiation (IR) for the indicated proteins. RAD51-positive cells are highlighted by the white arrowheads. The scale bar represents 5 μm.

(D–G) Quantification of confocal images, plotted as a box and whiskers plot. The box represents the 25th to 75th percentiles, and the whiskers show the minimum to maximum values. The experiment was performed at least twice, and data are plotted as a percentage of γH2AX- (D), 53BP1- (E), or RIF1-positive cells (> 10 foci) (F) or RAD51-positive cells (> 5 foci) (G) per field. Statistics were performed by Kruskal-Wallis non-parametric test followed by Dunn's multiple comparisons test. The indicated cell lines were compared with sgNT-treated cells (****$p < 0.0001$).

See also Figure S3.

Panier and Boulton, 2014). It was previously shown that the end resection defect in BRCA1-deficient cells can be rescued via loss of 53BP1, and this also rescued cell lethality induced by BRCA1 loss (Bouwman et al., 2010; Bunting et al., 2012). Hence, the finding that loss of the CST complex (Figure 3A) rescued BRCA1 lethality points toward a potential inhibitory role in DSB end resection. Moreover, depletion of CTC1 did not induce PARPi resistance in BRCA2-deficient cells (Figures S2A and S2B), which is in line with a possible role of the CST complex upstream of BRCA2.

DSB end resection produces ssDNA overhangs, which are protected from nucleolytic degradation and the formation of secondary structures by the coating of RPA. Therefore, we visualized RPA loading in response to α-particle-induced DNA damage by immunofluorescence as a readout for end resection (Stap et al., 2008). In line with previous studies (Tkáč et al., 2016; Xu et al., 2015), KB1P-G3 tumor cells showed a clear resection defect that was partially restored in *Ctc1*-mutated KB1P-G3 cells but not in sgNT-transfected control cells (Figures 4A and 4B).

We next investigated whether CTC1 loss affects the recruitment of DDR factors to sites of irradiation-induced DNA damage. CRISPR/SpCas9-targeted KB1P-G3 cells were either left untreated or treated with 10 Gy of IR, which potently induced

yH2AX foci (Figures 4C and 4D; Figures S3A and S3B). Although depletion of 53BP1 in KB1P-G3 cells abolished the formation of IR-induced 53BP1 and RIF1 foci, these effects were not observed in CTC1-depleted cells (Figures 4E and 4F and S3C and S3D). Despite the capacity to form 53BP1 and RIF1 foci, KB1P-G3 cells that were depleted of CTC1 restored IR-induced RAD51 focus formation, whereas sgNT-transfected control cells were deficient for this activity (Figures 4G and S3E). Similar conclusions were obtained when DNA damage was induced by treatment with 500 nM olaparib for 24 hr (Figures S3A and S3F–S3M). As expected, PARPi treatment resulted in more heterogeneous DNA damage induction compared with IR because PARP inhibition primarily exerts its cytotoxic effects during replication.

We then tested whether CTC1 loss resulted in productive HR events in conditional BRCA1-deficient $R26^{CreERT2}$;$Brca1^{SCo/\Delta}$;$Pim1^{DR\text{-}GFP/wt}$ mESC cells carrying a stably integrated DR-GFP reporter (Bouwman et al., 2013). These cells were transfected to transiently express mCherry and I-*Sce*I, and the percentage of mCherry/GFP double-positive cells was quantified by fluorescence-activated cell sorting (FACS) 24 hr later. Switching of the conditional $Brca1^{SCo}$ allele impaired HR activity, which was partially rescued upon depletion of the CST complex (Figures S3N and S3O).

Together, these data support a role for CTC1 as a resection antagonist acting on non-telomeric DSBs and as a mediator of the HR defect in BRCA1-deficient cells.

CTC1 Facilitates c-NHEJ-Mediated Repair at Telomeric and Non-Telomeric DSBs

It was previously shown that 53BP1, RIF1, and REV7/MAD2L2 antagonize resection and promote c-NHEJ (Boersma et al., 2015; Bouwman et al., 2010; Bunting et al., 2010; Chapman et al., 2013; Di Virgilio et al., 2013; Escribano-Díaz et al., 2013; Xu et al., 2015; Zimmermann et al., 2013). However, this is not a universal phenotype for resection antagonists because it is not shared by HELB (Tkáč et al., 2016). We therefore sought to determine whether CTC1 affects NHEJ activity. First, we used $Terf2^{-/-}$;$Trp53^{-/-}$ mouse embryonic fibroblasts (MEFs) that express a temperature-sensitive $TRF2^{Ile468Ala}$ mutant (TRF2ts) (Konishi and de Lange, 2008). TRF2ts is functional and maintains intact TRF2-protected telomeres at 32°C, but it dissociates from telomeres at 37°C–39°C, inducing a DDR response and end-to-end chromosome fusions (Konishi and de Lange, 2008). It was previously demonstrated that these fusions are driven by c-NHEJ and can be rescued by depletion of RNF8, DNA ligase IV, or REV7/MAD2L2 (Boersma et al., 2015; Celli and de Lange, 2005; Peuscher and Jacobs, 2011; Smogorzewska et al., 2002).

We depleted CTC1 in TRF2ts MEFs grown under permissive conditions (Figure 5A), which did not affect cell cycle distribution (Figures S4A and S4B). Cells were then grown at the non-permissive temperature (39°C) for 24 h to uncap telomeres and induce a DDR response prior to harvesting metaphase spreads for telomere fluorescence *in situ* hybridization (FISH). Although chromosome fusions were readily observed in control cells upon temperature-induced TRF2 inactivation, this was significantly reduced in *Ctc1*-mutated cells (Figures 5B and 5C; Figures S4C–S4E). In line with this finding and with NHEJ being inhibited by long ssDNA overhangs, it was previously shown that depletion of CTC1 increased ssG overhang length (Chen et al., 2012; Gu et al., 2012).

We next assessed whether CTC1 depletion in mouse CH12 B cells affects the ability to undergo class switch recombination (CSR) as a measure for non-telomeric c-NHEJ capacity (Muramatsu et al., 2000). CH12 cells were transfected with *Ctc1*-targeting CRISPR/SpCas9 constructs and subcloned to obtain *Ctc1*-mutated CH12 cell clones. Notably, only 2 of 96 tested clones showed heterozygous *Ctc1* allele disruption, and no homozygous knockouts were obtained (Figures S4F and S4G), raising the possibility that complete loss of CTC1 is lethal in CH12 cells. Wild-type and heterozygous *Ctc1* knockout clones were subsequently stimulated with CD40Ab, interleukin-4 (IL-4), and transforming growth factor β-1 (TGF-β-1, CD40Ab, IL-4, and TGFβ-1 [CIT]) to induce CSR from immunoglobulin M (IgM) to IgA, which was monitored by flow cytometry. Interestingly, heterozygous knockout of *Ctc1* significantly diminished CSR in both clones (Figures 5D and 5E). We therefore conclude that CTC1 facilitates DSB repair via c-NHEJ at both telomeric and non-telomeric regions.

Depletion of CTC1 Mediates PARPi Resistance in the KB1P Mouse Model

Last, we explored the *in vivo* effects of CTC1 on the treatment response of BRCA1-deficient tumors to PARP inhibition. We analyzed whether *Ctc1* mRNA expression levels were altered in our previously generated collection of BRCA1- and p53-deficient KB1P and KB1PM mouse mammary tumors with acquired resistance to PARP inhibition (Jaspers et al., 2013). In total, this collection comprises 60 treatment-naive tumors and 85 matched PARPi-resistant tumors derived from 23 unique donors. To examine the expression levels of *Ctc1* in treatment-naive and PARPi-resistant tumors, we produced RNA sequencing (RNA-seq) data for all tumors (E.G., unpublished data) and obtained the normalized expression values using edgeR (Robinson et al., 2010). We observed that the expression of *Ctc1* is significantly downregulated in PARPi-resistant tumors compared with naive tumors ($p = 6.34 \times 10^{-4}$) (Figure 6A). Moreover, in tumors for which copy number variation by sequencing (CNVseq) data were available, CTC1 mRNA downregulation correlated with CNV loss (Figures S5A and S5D). Although a similar correlation was observed for STN1 and TEN1, these factors were not significantly downregulated in resistant tumors (Figures S5B, S5C, S5E, and S5F).

Finally, we used mammary tumor organoid technology (Duarte et al., 2018) to perform an *in vivo* intervention study with the PARPi olaparib in mice carrying tumors derived from isogenic KB1P organoids with or without disruption of *Ctc1*. For this purpose, KB1P4 organoids, derived from a KB1P mammary tumor, were cultured *ex vivo* and co-transduced with lentiviruses produced from pCMV-SpCas9 and pLenti-sg*Ctc1*-tetR-T2A-Puro vectors. Control organoids were generated by co-transduction with pCMV-SpCas9 and pLenti-sgNT-tetR-T2A-Puro lentivirus encoding a non-targeting sgRNA (Figure 6B). The transduced KB1P4 tumor organoids were orthotopically transplanted in mice that were left untreated or treated daily with the PARPi olaparib for 56 consecutive days when tumors reached a size

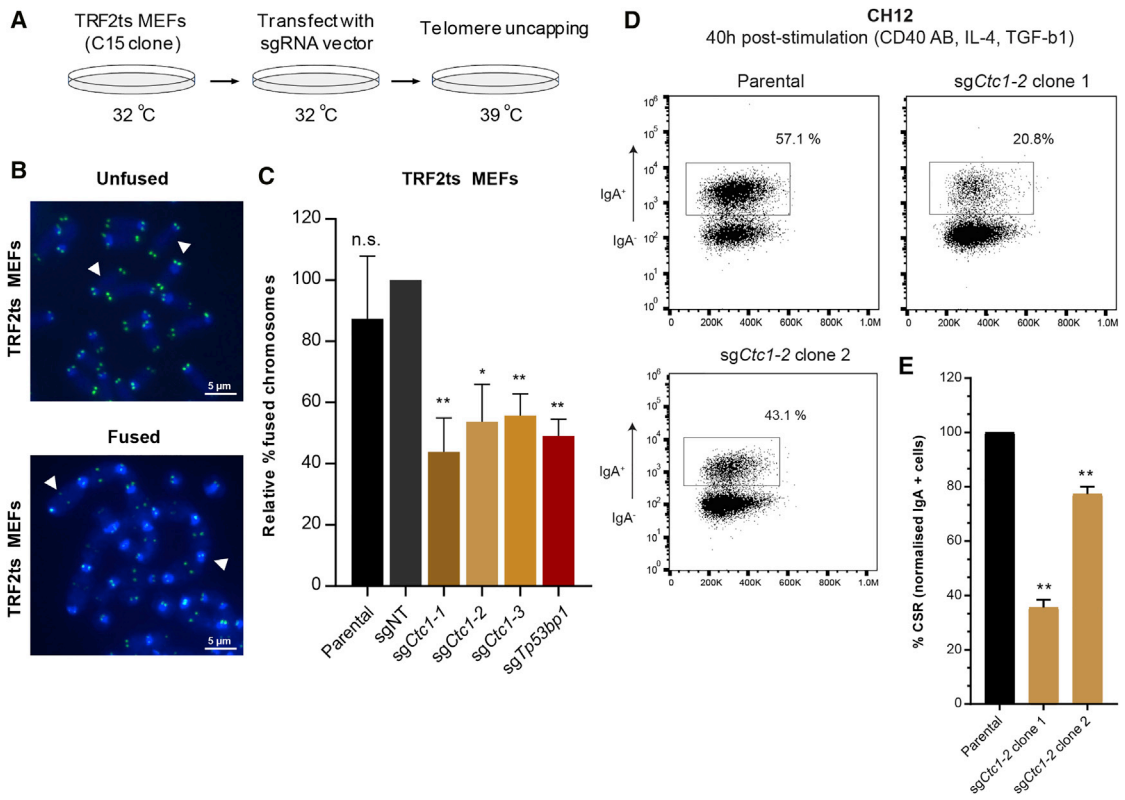

Figure 5. CTC1 Facilitates c-NHEJ at Telomeric and Non-telomeric DSBs

(A–C) CTC1 depletion suppresses end-to-end fusions of uncapped telomeres.

(A) Schematic overview of the telomere fusion assay. TRF2ts mouse embryonic fibroblasts (MEFs) of the indicated genotypes were cultured at the non-permissive temperature (39°C) for 24 hr before harvesting.

(B) Representative images of metaphase spreads showing chromosomes unfused or fused at their telomeres (examples highlighted by white arrowheads). Chromosomes were stained with DAPI and a telomere-specific FISH probe (green).

(C) Metaphases were detected and imaged automatically by Metafer. At least two independent experiments were performed, in each independent experiment, more than 2,000 chromosomes were counted manually. Genotypes were blinded during counting. Data are plotted as mean ± SEM. Significance was determined by unpaired two-tailed Student's t test (*$p \leq 0.05$; **$p \leq 0.01$).

(D and E) Heterozygous inactivation of *Ctc1* impairs IgM-to-IgA class switch recombination (CSR) in CH12 B cells.

(D) FACS analysis of CH12 clones of the indicated genotype 40 hr after induction of CSR by incubation with CD40Ab, IL-4, and TGF-β-1 (CIT).

(E) Quantification of FACS data, representing mean ± SD of two independent experiments. Significance was calculated by unpaired Student's t test (**p value ≤ 0.01).

of 50–100 mm^3. As expected, the *Ctc1* target site was efficiently disrupted in tumors derived from KB1P4 organoids transduced with pCMV-SpCas9 and pLenti-sg*Ctc1*-tetR-T2A-Puro (Figures 6C and 6D). Although KB1P4 control tumors only relapsed after treatment was stopped, CTC1-depleted tumors relapsed during treatment, resulting in accelerated mammary tumor-related death (median latencies: 39 days for sg*Ctc1_2* and 42 days for sg*Ctc1_3* cohorts compared with 73 days for control animals; log rank test, p = 0.0019 and p = 0.0086, respectively; Figure 6E). These data confirmed that depletion of CTC1 confers PARPi resistance in BRCA1-deficient tumors *in vivo*.

DISCUSSION

In this study, we show that loss of the CST complex members CTC1, STN1, and TEN1 induces PARPi resistance in tumors with irreversible loss of function of BRCA1. Our data highlight the CST complex as a pathway for tumor cells to escape the synthetic lethal effects of PARPi by restoring HR independently of BRCA1. In particular, we demonstrate that the underlying mechanism is a restoration of end resection of DSBs. Together, our findings demonstrate that the CST complex contributes to the regulation of DNA end stability not only at telomeres but also at non-telomeric DSBs.

We and others have recently shown that the 53BP1-RIF1-REV7/MAD2L2 pathway is crucial for blocking end resection of DSBs (Boersma et al., 2015; Bouwman et al., 2010; Bunting et al., 2010; Chapman et al., 2013; Di Virgilio et al., 2013; Escribano-Díaz et al., 2013; Xu et al., 2015; Zimmermann et al., 2013). However, it has remained elusive how DNA end stability is regulated by 53BP1-RIF1-REV7/MAD2L2 because none of these factors have been shown to contain direct DNA binding capacity and do not contain DNA processing activities. Our finding that the CST complex functions as a resection antagonist at

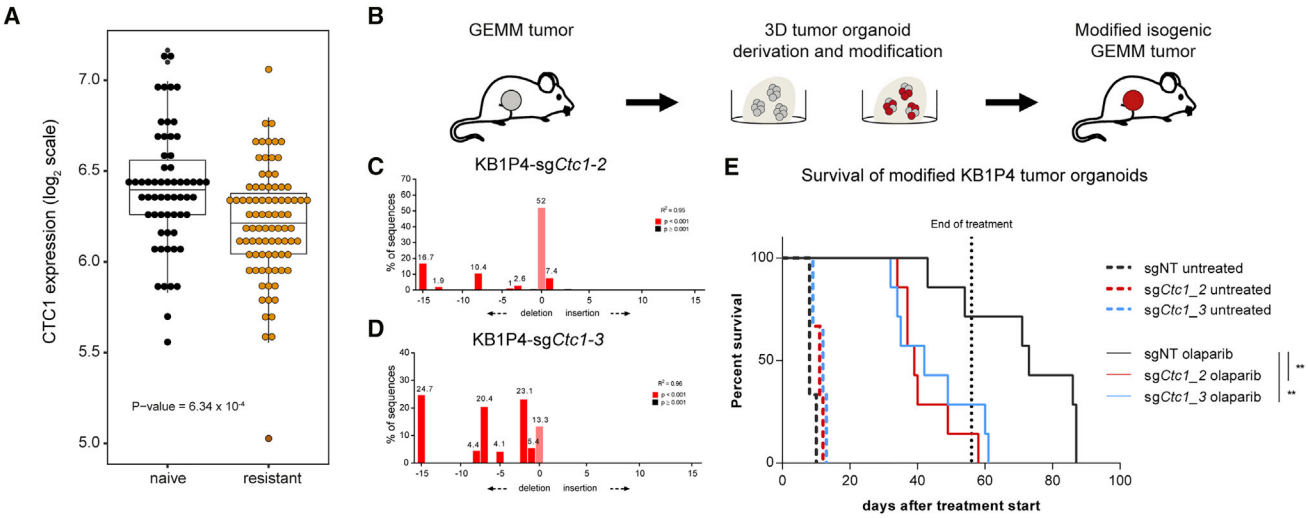

Figure 6. Depletion of CTC1 Induces PARP Inhibitor Resistance *In Vivo*

(A) mRNA expression levels of Ctc1 in matched treatment-naive and PARPi-resistant BRCA1-deficient mouse mammary tumors. The y axis indicates the log2 (counts per million) value.

(B) Schematic overview of the generation of isogenic Ctc1-mutated and control tumors via *ex vivo* manipulation of tumor organoids.

(C and D) Example TIDE plots of untreated mammary tumors derived from Ctc1-mutated KB1P4 tumor organoids of the indicated genotype.

(E) Survival of mice orthotopically transplanted with modified KB1P4 tumor organoids. Mice were stratified into untreated (n = 3) or olaparib-treated (100 mg/kg intraperitoneally daily for 56 consecutive days, n = 7) groups when tumors reached a size of 50–100 mm3. Significance was calculated by log rank (Mantel-Cox) test (**p < 0.01).

DSBs sheds light on this puzzle. The CST complex is an RPA-like complex that can directly bind ssDNA via multiple OB folds (Miyake et al., 2009). In collaboration with the laboratory of Dan Durocher, we recently identified another RPA-like complex, the Shieldin (SHLD) complex, which is composed of SHLD1 (C20ORF196), SHLD2 (FAM35A), SHLD3 (FLJ26957/CTC-534A2.2), and REV7/MAD2L2, as a downstream effector of 53BP1 in DSB repair (unpublished data). Hence, in addition to RPA and the SHLD complex, the CST complex is another trimeric complex that contains direct DNA binding capacity and affects DSB end stability. How these three complexes are recruited to DSBs in time and space remains to be elucidated. Possibly, RPA, SHLD, and CST compete for ssDNA at resected DSBs or collapsed forks to either promote or antagonize HR. Not mutually exclusive with this model, it is conceivable that these complexes might contain specialized functions dependent on the ssDNA substrate since the CST complex has been reported to preferentially bind to and promote melting of G-rich regions and G4-quadruplexes (Bhattacharjee et al., 2017; Lue et al., 2013).

Future work is also required to elucidate whether these complexes form the final step in the regulation of DSB end stability (for instance, through steric hindrance) or whether additional downstream factors are involved. Intriguingly, the CST complex has been described to buffer resection at telomeres via POLA-dependent fill-in DNA synthesis, which is required to prevent excessive telomere erosion (Lazzerini-Denchi and Sfeir, 2016). Our finding that the CST complex antagonizes resection at non-telomeric DSBs raises the question of whether this is dependent on POLA activity. Resection can possibly be antagonized not only by shielding the ends of DSBs from end-processing activities but also by directly counteracting ongoing resection via fill-in DNA synthesis. This buffering activity might fine-tune the length of ssDNA around the DSB, which is vulnerable for nucleolytic degradation, and it might provide a rescue mechanism in case HR cannot be completed.

The identification of the CST complex as a mediator of PARPi response in BRCA1-deficient tumors might also have clinical implications because loss-of-function mutations in the CST-encoding genes are predicted to cause clinical PARPi resistance. Moreover, we expect that these alterations provide therapeutic vulnerabilities because we recently found that depletion of the 53BP1-dependent DNA repair pathway enhances sensitivity to IR (M.B., unpublished data).

EXPERIMENTAL PROCEDURES

Cell Culture and Gene Editing

The KB1P-G3 cell line was previously established from a *K14cre;Brca1$^{F/F}$;Trp53$^{F/F}$* (KB1P) mouse mammary tumor and cultured as described by Jaspers et al. (2013). The KB2P-3.4 cell line was previously established from a *K14cre;Brca2$^{F/F}$;Trp53$^{F/F}$* (KB2P) mouse mammary tumor and cultured as described by Evers et al. (2008). The KB1P4 3D tumor organoid line was previously established from a *Brca1$^{-/-}$;p53$^{-/-}$* mouse mammary tumor and cultured as described by Duarte et al. (2018). Further *in vitro* culture details and gene editing details are provided in the Supplemental Experimental Procedures.

Plasmids

Plasmids and cloning methods are provided in the Supplemental Experimental Procedures.

PARPis

Olaparib (CAS 763113-22-0) and AZD2461 (CAS 1174043-16-3) were synthesized by and purchased from Syncom (Groningen, the Netherlands). Talazoparib was purchased from Selleckchem (catalog no.S7048).

Genomic DNA Isolation, PCR Amplification, and TIDE Analysis

Allele modification frequencies were quantified from genomic DNA isolated from tumor and cell line samples using Gentra Puregene (QIAGEN) according to the manufacturer's protocol. Target loci were amplified by PCR and submitted for Sanger sequencing to confirm target modification using the TIDE algorithm (Brinkman et al., 2014). Parental cells were used as a reference sequence. PCR primer sequences are provided in Table S3. Further details are provided in the Supplemental Experimental Procedures.

CRISPR Library Screens

Screening details are provided in the Supplemental Experimental Procedures.

Alpha Track Assay

Experiments were performed as described previously (Xu et al., 2015) with minor modifications. Details are provided in the Supplemental Experimental Procedures.

Focus Formation Experiments

RAD51 immunofluorescence in CRISPR/SpCas9-transfected KB1P-G3 cells was performed as described previously with minor modifications (Xu et al., 2015). Details are provided in the Supplemental Experimental Procedures.

DR-GFP

The DR-GFP was performed as described previously (Bouwman et al., 2013). Genes were targeted using the pLentiCRISPRv2 system containing the indicated sgRNAs.

Assessment of Telomere NHEJ

Trf2$^{-/-}$;*Trp53*$^{-/-}$;TRF2ts (TRF2ts) MEFs were described before (Peuscher and Jacobs, 2011), and metaphase chromosome analysis was done as described before (Boersma et al., 2015). Details are provided in the Supplemental Experimental Procedures.

CSR Assay

Immunoglobulin CSR was performed as described previously (Xu et al., 2015). Details are provided in the Supplemental Experimental Procedures.

Generation of RNA-Seq Data

To determine the effects of Ctc1, Ten1, and Stn1 on PARPi treatment *in vivo*, we used our RNA-seq dataset generated from a cohort of PARPi-naive and -resistant KB1P and KB1PM tumors (Jaspers et al., 2013; E.G., unpublished data). Further details are provided in the Supplemental Experimental Procedures.

Generation of CNV Sequencing Data

Genomic DNA was isolated from a subset of matched naive-and resistant KB1P-derived fresh-frozen tumor material using standard phenol:chloroform extraction (Jaspers et al., 2013; E.G., unpublished data). Further details are provided in the Supplemental Experimental Procedures.

In Vivo Studies

All animal experiments were approved by the Animal Ethics Committee of the Netherlands Cancer Institute (Amsterdam, the Netherlands) and performed in accordance with the Dutch Act on Animal Experimentation (November 2014). Tumor organoids were allografted in 6- to 9-week-old female mice as described previously (Duarte et al., 2018) with minor modifications. Further details are provided in the Supplemental Experimental Procedures.

Quantification and Statistical Analysis

Statistical differences were calculated in GraphPad Prism using Student's t tests. Statistical significance in Figure 2F was calculated by two-way ANOVA and *post hoc* Dunnett's correction for multiple comparisons and in Figure 2G by one-way ANOVA and *post hoc* Dunnett's correction for multiple comparisons. Statistical differences in Figures 4D–4G and Figures S3F–S3M were calculated by Kruskal-Wallis non-parametric test and *post hoc* Dunnett's correction for multiple comparisons. Statistical differences in Figure 6E were calculated by log rank Mantel-Cox test. Significance is as follows: $p > 0.05$, not significant (n.s.); $^{*}p \leq 0.05$; $^{**}p \leq 0.01$; $^{***}p \leq 0.001$; $^{****}p \leq 0.0001$ unless otherwise stated in the figure legends. Original data files used to prepare the figures in this manuscript have been deposited in Mendeley Data and are available at https://doi.org/10.17632/6wyzgw8z8k.1.

Contact for Reagent and Resource Sharing

Further information and requests for resources and reagents should be directed to and will be fulfilled by S.R. (sven.rottenberg@vetsuisse.unibe.ch).

DATA AND SOFTWARE AVAILABILITY

The accession number for the raw data of RNA-seq and CNV sequencing reported in this paper is European Nucleotide Archive (ENA): PRJEB25803.

SUPPLEMENTAL INFORMATION

Supplemental Information includes Supplemental Experimental Procedures, five figures, and three tables and can be found with this article online at https://doi.org/10.1016/j.celrep.2018.04.046.

ACKNOWLEDGMENTS

We wish to thank Piet Borst for critical reading of the manuscript, the members of the Preclinical Intervention Unit of the Mouse Clinic for Cancer and Aging (MCCA) at the Netherlands Cancer Institute (NKI) for their technical support with the animal experiments, and Julian R. de Ruiter for assistance with bioinformatic analysis. We are grateful to the NKI animal facility, digital microscopy facility, flow cytometry facility, and genomics core facility for their excellent service. Financial support came from the Dutch Cancer Society (KWF 2011-5220 and 2014-6532 to S.R. and J.J.), the Netherlands Organization for Scientific Research (VICI 91814643, NGI 93512009, Cancer Genomics Netherlands, and a National Roadmap Grant for Large-Scale Research Facilities to J.J. and STW 13577 to D.C.v.G.), the Swiss National Science Foundation (310030_156869 to S.R.), the Swiss Cancer League (KLS-4282-08-2017 to S.R.), the European Union (ERC StG 311565 to J.J.L.J., ERC CoG-681572 to S.R., and ERC Synergy Grant 319661 to J.J.), Cancer Research UK (CRUK/A14276 to C.J.L.), and a Breast Cancer Now Program Grant (CTR-Q4-Y2 to C.J.L.). R.C. and H.G. are supported by Cancer Research UK (C52690/A19270) and MRC (MR/M009971/1) grants, respectively, and a Wellcome core award (090532/Z/09/Z).

AUTHOR CONTRIBUTIONS

Conceptualization, M.B., J.J., and S.R.; Methodology; M.B., S.A., S.J.P., B.E., and J.B.; Software and Formal Analysis, M.B., J.B., J.J., and S.R.; Investigation, M.B., S.A., S.J.P., I.d.K., H.G., S.J.R., C.L., J.F., F.F.S., and R.B.; Resources; B.E. and E.G.; Writing, M.B., J.J., and S.R.; Supervision, M.v.d.V., D.C.v.G., J.J.L.J., R.C., C.J.L., J.J., and S.R.; Funding Acquisition, D.C.v.G., J.J.L.J., R.C., C.J.L., J.J., and S.R.

DECLARATION OF INTERESTS

C.J.L. is a named inventor on patents describing the use of PARPis and stands to gain as part of the ICR's "Rewards to Investors" scheme.

Received: January 31, 2018
Revised: March 24, 2018
Accepted: April 11, 2018
Published: May 15, 2018

REFERENCES

Bhattacharjee, A., Wang, Y., Diao, J., and Price, C.M. (2017). Dynamic DNA binding, junction recognition and G4 melting activity underlie the telomeric and genome-wide roles of human CST. Nucleic Acids Res. *45*, 12311–12324.

Boersma, V., Moatti, N., Segura-Bayona, S., Peuscher, M.H., van der Torre, J., Wevers, B.A., Orthwein, A., Durocher, D., and Jacobs, J.J.L. (2015). MAD2L2 controls DNA repair at telomeres and DNA breaks by inhibiting 5′ end resection. Nature *521*, 537–540.

Bouwman, P., Aly, A., Escandell, J.M., Pieterse, M., Bartkova, J., van der Gulden, H., Hiddingh, S., Thanasoula, M., Kulkarni, A., Yang, Q., et al. (2010). 53BP1 loss rescues BRCA1 deficiency and is associated with triple-negative and BRCA-mutated breast cancers. Nat. Struct. Mol. Biol. *17*, 688–695.

Bouwman, P., van der Gulden, H., van der Heijden, I., Drost, R., Klijn, C.N., Prasetyanti, P., Pieterse, M., Wientjens, E., Seibler, J., Hogervorst, F.B., and Jonkers, J. (2013). A high-throughput functional complementation assay for classification of BRCA1 missense variants. Cancer Discov. *3*, 1142–1155.

Brinkman, E.K., Chen, T., Amendola, M., and van Steensel, B. (2014). Easy quantitative assessment of genome editing by sequence trace decomposition. Nucleic Acids Res. *42*, e168.

Bunting, S.F., Callén, E., Wong, N., Chen, H.T., Polato, F., Gunn, A., Bothmer, A., Feldhahn, N., Fernandez-Capetillo, O., Cao, L., et al. (2010). 53BP1 inhibits homologous recombination in Brca1-deficient cells by blocking resection of DNA breaks. Cell *141*, 243–254.

Bunting, S.F., Callén, E., Kozak, M.L., Kim, J.M., Wong, N., López-Contreras, A.J., Ludwig, T., Baer, R., Faryabi, R.B., Malhowski, A., et al. (2012). BRCA1 functions independently of homologous recombination in DNA interstrand crosslink repair. Mol. Cell *46*, 125–135.

Celli, G.B., and de Lange, T. (2005). DNA processing is not required for ATM-mediated telomere damage response after TRF2 deletion. Nat. Cell Biol. *7*, 712–718.

Chapman, J.R., Barral, P., Vannier, J.B., Borel, V., Steger, M., Tomas-Loba, A., Sartori, A.A., Adams, I.R., Batista, F.D., and Boulton, S.J. (2013). RIF1 is essential for 53BP1-dependent nonhomologous end joining and suppression of DNA double-strand break resection. Mol. Cell *49*, 858–871.

Chen, L.Y., Redon, S., and Lingner, J. (2012). The human CST complex is a terminator of telomerase activity. Nature *488*, 540–544.

Daley, J.M., and Sung, P. (2014). 53BP1, BRCA1, and the choice between recombination and end joining at DNA double-strand breaks. Mol. Cell. Biol. *34*, 1380–1388.

Di Virgilio, M., Callen, E., Yamane, A., Zhang, W., Jankovic, M., Gitlin, A.D., Feldhahn, N., Resch, W., Oliveira, T.Y., Chait, B.T., et al. (2013). Rif1 prevents resection of DNA breaks and promotes immunoglobulin class switching. Science *339*, 711–715.

Duarte, A.A., Gogola, E., Sachs, N., Barazas, M., Annunziato, S., R de Ruiter, J., Velds, A., Blatter, S., Houthuijzen, J.M., van de Ven, M., et al. (2018). BRCA-deficient mouse mammary tumor organoids to study cancer-drug resistance. Nat. Methods *15*, 134–140.

Elstrodt, F., Hollestelle, A., Nagel, J.H., Gorin, M., Wasielewski, M., van den Ouweland, A., Merajver, S.D., Ethier, S.P., and Schutte, M. (2006). BRCA1 mutation analysis of 41 human breast cancer cell lines reveals three new deleterious mutants. Cancer Res. *66*, 41–45.

Escribano-Díaz, C., Orthwein, A., Fradet-Turcotte, A., Xing, M., Young, J.T., Tkáč, J., Cook, M.A., Rosebrock, A.P., Munro, M., Canny, M.D., et al. (2013). A cell cycle-dependent regulatory circuit composed of 53BP1-RIF1 and BRCA1-CtIP controls DNA repair pathway choice. Mol. Cell *49*, 872–883.

Evers, B., Drost, R., Schut, E., de Bruin, M., van der Burg, E., Derksen, P.W., Holstege, H., Liu, X., van Drunen, E., Beverloo, H.B., et al. (2008). Selective inhibition of BRCA2-deficient mammary tumor cell growth by AZD2281 and cisplatin. Clin. Cancer Res. *14*, 3916–3925.

Feng, L., Li, N., Li, Y., Wang, J., Gao, M., Wang, W., and Chen, J. (2015). Cell cycle-dependent inhibition of 53BP1 signaling by BRCA1. Cell Discov. *1*, 15019.

Feng, X., Hsu, S.J., Kasbek, C., Chaiken, M., and Price, C.M. (2017). CTC1-mediated C-strand fill-in is an essential step in telomere length maintenance. Nucleic Acids Res. *45*, 4281–4293.

Gu, P., Min, J.N., Wang, Y., Huang, C., Peng, T., Chai, W., and Chang, S. (2012). CTC1 deletion results in defective telomere replication, leading to catastrophic telomere loss and stem cell exhaustion. EMBO J. *31*, 2309–2321.

Hom, R.A., and Wuttke, D.S. (2017). Human CST Prefers G-Rich but Not Necessarily Telomeric Sequences. Biochemistry *56*, 4210–4218.

Jaspers, J.E., Kersbergen, A., Boon, U., Sol, W., van Deemter, L., Zander, S.A., Drost, R., Wientjens, E., Ji, J., Aly, A., et al. (2013). Loss of 53BP1 causes PARP inhibitor resistance in Brca1-mutated mouse mammary tumors. Cancer Discov. *3*, 68–81.

Koike-Yusa, H., Li, Y., Tan, E.P., Velasco-Herrera, Mdel.C., and Yusa, K. (2014). Genome-wide recessive genetic screening in mammalian cells with a lentiviral CRISPR-guide RNA library. Nat. Biotechnol. *32*, 267–273.

Konishi, A., and de Lange, T. (2008). Cell cycle control of telomere protection and NHEJ revealed by a ts mutation in the DNA-binding domain of TRF2. Genes Dev. *22*, 1221–1230.

Lazzerini-Denchi, E., and Sfeir, A. (2016). Stop pulling my strings - what telomeres taught us about the DNA damage response. Nat. Rev. Mol. Cell Biol. *17*, 364–378.

Li, W., Xu, H., Xiao, T., Cong, L., Love, M.I., Zhang, F., Irizarry, R.A., Liu, J.S., Brown, M., and Liu, X.S. (2014). MAGeCK enables robust identification of essential genes from genome-scale CRISPR/Cas9 knockout screens. Genome Biol. *15*, 554.

Liu, X., Holstege, H., van der Gulden, H., Treur-Mulder, M., Zevenhoven, J., Velds, A., Kerkhoven, R.M., van Vliet, M.H., Wessels, L.F., Peterse, J.L., et al. (2007). Somatic loss of BRCA1 and p53 in mice induces mammary tumors with features of human BRCA1-mutated basal-like breast cancer. Proc. Natl. Acad. Sci. USA *104*, 12111–12116.

Lord, C.J., and Ashworth, A. (2017). PARP inhibitors: Synthetic lethality in the clinic. Science *355*, 1152–1158.

Lue, N.F., Zhou, R., Chico, L., Mao, N., Steinberg-Neifach, O., and Ha, T. (2013). The telomere capping complex CST has an unusual stoichiometry, makes multipartite interaction with G-Tails, and unfolds higher-order G-tail structures. PLoS Genet. *9*, e1003145.

Makarov, V.L., Hirose, Y., and Langmore, J.P. (1997). Long G tails at both ends of human chromosomes suggest a C strand degradation mechanism for telomere shortening. Cell *88*, 657–666.

Mateo, J., Carreira, S., Sandhu, S., Miranda, S., Mossop, H., Perez-Lopez, R., Nava Rodrigues, D., Robinson, D., Omlin, A., Tunariu, N., et al. (2015). DNA-repair defects and Olaparib in metastatic prostate cancer. N. Engl. J. Med. *373*, 1697–1708.

McElligott, R., and Wellinger, R.J. (1997). The terminal DNA structure of mammalian chromosomes. EMBO J. *16*, 3705–3714.

Miyake, Y., Nakamura, M., Nabetani, A., Shimamura, S., Tamura, M., Yonehara, S., Saito, M., and Ishikawa, F. (2009). RPA-like mammalian Ctc1-Stn1-Ten1 complex binds to single-stranded DNA and protects telomeres independently of the Pot1 pathway. Mol. Cell *36*, 193–206.

Muramatsu, M., Kinoshita, K., Fagarasan, S., Yamada, S., Shinkai, Y., and Honjo, T. (2000). Class switch recombination and hypermutation require activation-induced cytidine deaminase (AID), a potential RNA editing enzyme. Cell *102*, 553–563.

Oplustil O'Connor, L., Rulten, S.L., Cranston, A.N., Odedra, R., Brown, H., Jaspers, J.E., Jones, L., Knights, C., Evers, B., Ting, A., et al. (2016). The PARP inhibitor AZD2461 provides insights into the role of PARP3 inhibition for both synthetic lethality and tolerability with chemotherapy in preclinical models. Cancer Res. *76*, 6084–6094.

Panier, S., and Boulton, S.J. (2014). Double-strand break repair: 53BP1 comes into focus. Nat. Rev. Mol. Cell Biol. *15*, 7–18.

Patch, A.M., Christie, E.L., Etemadmoghadam, D., Garsed, D.W., George, J., Fereday, S., Nones, K., Cowin, P., Alsop, K., Bailey, P.J., et al.; Australian Ovarian Cancer Study Group (2015). Whole-genome characterization of chemoresistant ovarian cancer. Nature *521*, 489–494.

Pettitt, S.J., Krastev, D.B., Brandsma, I., Drean, A., Song, F., Aleksandrov, R., Harrell, M.I., Menon, M., Brough, R., Campbell, J., *et al*. (2017).

Peuscher, M.H., and Jacobs, J.J. (2011). DNA-damage response and repair activities at uncapped telomeres depend on RNF8. Nat. Cell Biol. *13*, 1139–1145.

Prahallad, A., Heynen, G.J., Germano, G., Willems, S.M., Evers, B., Vecchione, L., Gambino, V., Lieftink, C., Beijersbergen, R.L., Di Nicolantonio, F., et al. (2015). PTPN11 Is a Central Node in Intrinsic and Acquired Resistance to Targeted Cancer Drugs. Cell Rep. *12*, 1978–1985.

Pritchard, C.C., Mateo, J., Walsh, M.F., De Sarkar, N., Abida, W., Beltran, H., Garofalo, A., Gulati, R., Carreira, S., Eeles, R., et al. (2016). Inherited DNA-repair gene mutations in men with metastatic prostate cancer. N. Engl. J. Med. *375*, 443–453.

Robinson, M.D., McCarthy, D.J., and Smyth, G.K. (2010). edgeR: a Bioconductor package for differential expression analysis of digital gene expression data. Bioinformatics *26*, 139–140.

Rottenberg, S., Jaspers, J.E., Kersbergen, A., van der Burg, E., Nygren, A.O., Zander, S.A., Derksen, P.W., de Bruin, M., Zevenhoven, J., Lau, A., et al. (2008). High sensitivity of BRCA1-deficient mammary tumors to the PARP inhibitor AZD2281 alone and in combination with platinum drugs. Proc. Natl. Acad. Sci. USA *105*, 17079–17084.

Sfeir, A., and de Lange, T. (2012). Removal of shelterin reveals the telomere end-protection problem. Science *336*, 593–597.

Smogorzewska, A., Karlseder, J., Holtgreve-Grez, H., Jauch, A., and de Lange, T. (2002). DNA ligase IV-dependent NHEJ of deprotected mammalian telomeres in G1 and G2. Curr. Biol. *12*, 1635–1644.

Stap, J., Krawczyk, P.M., Van Oven, C.H., Barendsen, G.W., Essers, J., Kanaar, R., and Aten, J.A. (2008). Induction of linear tracks of DNA double-strand breaks by alpha-particle irradiation of cells. Nat. Methods *5*, 261–266.

Swisher, E.M., Sakai, W., Karlan, B.Y., Wurz, K., Urban, N., and Taniguchi, T. (2008). Secondary BRCA1 mutations in BRCA1-mutated ovarian carcinomas with platinum resistance. Cancer Res. *68*, 2581–2586.

Ter Brugge, P., Kristel, P., van der Burg, E., Boon, U., de Maaker, M., Lips, E., Mulder, L., de Ruiter, J., Moutinho, C., Gevensleben, H., et al. (2016). Mechanisms of Therapy Resistance in Patient-Derived Xenograft Models of BRCA1-Deficient Breast Cancer. J. Natl. Cancer Inst. *108*, djw148.

Tkáč, J., Xu, G., Adhikary, H., Young, J.T.F., Gallo, D., Escribano-Díaz, C., Krietsch, J., Orthwein, A., Munro, M., Sol, W., et al. (2016). HELB Is a Feedback Inhibitor of DNA End Resection. Mol. Cell *61*, 405–418.

Tzelepis, K., Koike-Yusa, H., De Braekeleer, E., Li, Y., Metzakopian, E., Dovey, O.M., Mupo, A., Grinkevich, V., Li, M., Mazan, M., et al. (2016). A CRISPR Dropout Screen Identifies Genetic Vulnerabilities and Therapeutic Targets in Acute Myeloid Leukemia. Cell Rep. *17*, 1193–1205.

Wang, Y., Bernhardy, A.J., Cruz, C., Krais, J.J., Nacson, J., Nicolas, E., Peri, S., van der Gulden, H., van der Heijden, I., O'Brien, S.W., et al.; kConFab Investigators (2016). The BRCA1-Δ11q Alternative Splice Isoform Bypasses Germline Mutations and Promotes Therapeutic Resistance to PARP Inhibition and Cisplatin. Cancer Res. *76*, 2778–2790.

Wang, G., Zimmermann, M., Mascall, K., Lenoir, W.F., Moffat, J., Angers, S., Durocher, D., and Hart, T. (2017). Identifying drug-gene interactions from CRISPR knockout screens with drugZ. bioRxiv. https://doi.org/10.1101/232736.

Wu, P., Takai, H., and de Lange, T. (2012). Telomeric 3′ overhangs derive from resection by Exo1 and Apollo and fill-in by POT1b-associated CST. Cell *150*, 39–52.

Xu, G., Chapman, J.R., Brandsma, I., Yuan, J., Mistrik, M., Bouwman, P., Bartkova, J., Gogola, E., Warmerdam, D., Barazas, M., et al. (2015). REV7 counteracts DNA double-strand break resection and affects PARP inhibition. Nature *521*, 541–544.

Zimmermann, M., Lottersberger, F., Buonomo, S.B., Sfeir, A., and de Lange, T. (2013). 53BP1 regulates DSB repair using Rif1 to control 5′ end resection. Science *339*, 700–704.